Heliyon 10 (2024) e27579

Contents lists available at ScienceDirect

Heliyon

journal homepage: www.cell.com/heliyon

Research article

Optimization of green silver nanoparticles as nanofungicides for management of rice bakanae disease

Quazi Shireen Akhter Jahan [a,1], Ziniya Sultana [b,1], Md. Asad Ud-Daula [b], Md. Ashikuzzaman [b], Md. Shamim Reja [b], Md. Mahfuzur Rahman [b], Amina Khaton [a], Md. Abul Kashem Tang [b], M. Safiur Rahman [c], Hossain Md. Faruquee [d], Seung Ju Lee [e,**], A.T.M. Mijanur Rahman [b,*]

[a] *Plant Pathology Division, Bangladesh Rice Research Institute, Gazipur, 1701, Bangladesh*
[b] *Department of Applied Nutrition and Food Technology, Islamic University, Kushtia, 7003, Bangladesh*
[c] *Chemistry Division, Atomic Energy Centre (AECD), Bangladesh Atomic Energy Commission, Bangladesh*
[d] *Department of Biotechnology and Genetical Engineering, Islamic University, Kushtia, 7003, Bangladesh*
[e] *Department of Food Science and Biotechnology, Dongguk University, Seoul, South Korea*

ARTICLE INFO

Keywords:
Green synthesis
Optimization
Silver nanoparticles
Nanofungicides
Fusarium species
Rice bakanae

ABSTRACT

Rice bakanae, a devastating seed-borne disease caused by *Fusarium* species requires a more attractive and eco-friendly management strategy. The optimization of plant-mediated silver nanoparticles (AgNPs) as nanofungicides by targeting *Fusarium* species may be a rational approach. In this study, *Azadirachta indica* leaf aqueous extract-based AgNPs (*Ai*LAE-AgNPs) were synthesized through the optimization of three reaction parameters: *A. indica* leaf amount, plant extract-to-$AgNO_3$ ratio (reactant ratio), and incubation time. The optimized green AgNPs were characterized using ultraviolet–visible light (UV–Vis) spectroscopy, field emission scanning electron microscopy (FESEM) with energy dispersive X-ray (EDX) spectroscopy, transmission electron microscopy (TEM), dynamic light scattering (DLS), and powder X-ray diffraction (XRD) techniques. The optimal conditions for producing spherical, unique, and diminutive-sized AgNPs ranging from 4 to 27 nm, with an average size of 15 nm, were 2 g *Ai*LAE at a 1:19 ratio (extract-to-$AgNO_3$) and incubated for 4 h. *Fusarium* isolates collected from infected soils and identified as *F. fujikuroi* (40) and *F. proliferatum* (58 and 65) by PCR were used for seed infestation. The AgNPs exhibited concentration-dependent mycelial growth inhibition with EC_{50} values ranging from 2.95 to 5.50 μg/mL. The AgNPs displayed exposure time-dependent seed disinfectant potential (complete CFU reduction in *F. fujikuroi* (40) and *F. proliferatum* (58) was observed at a concentration of 17.24 μg/mL). The optimized green AgNPs were non-toxic to germinating seeds, and completely cured bakanae under net-house conditions, suggesting their great nano-fungicidal potency for food security and sustainable agriculture.

* Corresponding author.
** Corresponding author.
E-mail addresses: Lseungju@dongguk.edu (S.J. Lee), mijan@anft.iu.ac.bd (A.T.M.M. Rahman).
[1] Q. Shireen Akhter Jahan[a] and Ziniya Sultana[b] have contributed equally to this work.

https://doi.org/10.1016/j.heliyon.2024.e27579
Received 13 February 2024; Received in revised form 29 February 2024; Accepted 1 March 2024
Available online 15 March 2024

1. Introduction

Bakanae, an extremely destructive seed-borne fungal disease of rice (*Oryza sativa* L.) caused by *Fusarium fujikuroi* species complex (FFCS), has been reported to cause yield losses of up to 95.4% under severe infection, depending on the region and variety. Among the FFSC, *F. fujikuroi, F. proliferatum, F. verticillioides* and *F. andiyazi* were the main pathogens responsible for rice bakanae [1]. Infected plants are typically thinner and taller than healthy plants and have yellowish-green or pale-green leaves. The abnormal production of the plant growth-promoting phytohormone, gibberellic acid (GA_3), by disease-causing pathogens is primarily responsible for the development of the classical symptoms [1]. Among the various tools used to manage Bakanae, seed treatment using chemical fungicides is the most effective and widely used. However, due to the misuse and overuse of chemical fungicides, phytopathogens have become resistant to this approach, negatively affecting rice productivity. In addition, excessive use of chemical fungicides in agricultural systems poses major concerns for public health and the environment [2]. Therefore, there is great interest in developing a more effective and environmentally safe management strategy that employs naturally active compounds for sustainable agricultural systems. The synthesis of nanofungicides via green routes, particularly using plant systems, may be a robust approach for controlling Bakanae disease.

Recently, plant extract-mediated silver nanoparticles (PEM-AgNPs), particularly nanofungicides, have been considered the best option for agricultural applications in the management of phytopathogenic microorganisms because of their advantages over other biological entities, such as faster synthesis of nanoparticles, simple and enhanced antifungal activities, cost-effectiveness, relatively easy scale-up, and eco-friendliness [3,4]**.** Various structurally and functionally diverse secondary metabolites naturally present in different parts of plants can act as reducing agents to convert Ag^{+} ions into AgNPs, facilitate their stabilization, improve physicochemical and biological properties, and reduce toxicity [5–8]. Another striking feature of AgNPs is that pathogenic microorganisms do not become resistant [9], which has led to AgNPs being considered potentially ideal fungicides for practical applications. Very small, monodisperse, and spherical AgNPs have been reported to have superior fungicidal potential owing to their high surface-to-volume ratio [2]. Therefore, it is of pivotal importance to generate PEM-AgNPs with the desired and controllable physicochemical properties for application as nanofungicides to protect crops. Optimization of the most important reaction parameters (plant extract-to-$AgNO_3$ ratios, concentration of $AgNO_3$, incubation times, pH, temperature, etc.) is key for the controlled biosynthesis of AgNPs [10,11] as well as the effective management of phytopathogens without exhibiting any toxic effects on non-target organisms [12]. Furthermore, maximum efficacy under field conditions can only be attained when AgNPs are optimized by targeting one specific crop species or a group of related crop species infected with similar phytopathogens [12].

The application of PEM-AgNPs under field conditions is the most recent advancement of nanotechnology in agro-ecosystems and has been gaining popularity among farmers owing to the overproduction of crops. One study [13] reported that treatment with *Azadirachta indica* leaf extract-based AgNPs (*Ai*LAE-AgNPs) is an eco-friendly and safe approach that significantly enhances the growth and yield of tomato plants by reducing the severity of early blight disease (caused by *Alternaria solani*). The positive outcome, notwithstanding, was that the reaction parameters were not optimized, which is one of the major limitations of this study. In a related study, Jo et al. (14) reported the *in vitro* antifungal and seed disinfection efficacies of chemically synthesized AgNPs against *G. fujikuroi*. To increase the fungicidal potential of AgNPs at very low concentrations, Sharma et al. (15) 1, 2, 4-triazolyldithiocarbamate-conjugated silver nanoparticles (TDTC-AgNPs) were synthesized and evaluated for their potential as a nanofungicide to manage rice bakanae disease under *in vitro* and field conditions. To prepare TDTC-AgNPs, 1,2,4-triazole was combined with dithiocarbamates (both potent chemical fungicides) to produce 1,2,4-triazole-1-ylcarbodithioate (TDTC), which was subsequently conjugated to chemically synthesized AgNPs. However, it was hypothesized that the optimized PEM-AgNPs would manage rice bakanae disease more efficiently and effectively without showing any toxic effects at a significantly lower dosage than chemically synthesized AgNPs alone or their conjugates. Therefore, the present study investigated the optimization and characterization of *Ai*LAE-AgNPs and, as a novel approach, evaluated their potential as nanofungicides against the targeted fungal pathogens, *Fusarium* sp. (isolated from the soils of bakanae-prone areas) under *in vitro* and net-house conditions.

A. indica (commonly known as neem) belongs to the Meliaceae family and is considered the best biocontrol agent in agriculture because of its low toxicity, availability, chemical diversity, potent secondary metabolites, and high efficacy against phytopathogens. Different parts of the plant possess important secondary metabolites; however, the leaves, in particular, are known to contain glycoproteins, triterpenes, polyphenols, saponins, and limonoids, such as azadirachtin, nimbolinin, nimbin, and nimbidin. Although Azadirachtin (a complex tetranortriterpenoid) is the main chemical compound responsible for the antimicrobial properties of *A. indica* leaves, polyphenols and other limonoids also have beneficial effects [14]. However, AgNPs biosynthesized using *Ai*LAE exhibited superior antifungal activity compared to the extract alone [15]. Various antimicrobial mechanisms have been proposed for AgNPs, including attachment to the surface of the cell wall and membrane, infiltration into the cell wall or membrane, interaction with cellular structures and biomolecules, generation of reactive oxygen species (ROS) and free radical species due to cellular toxicity and oxidative stress, and modulation of signal transduction pathways [16].

In this study, three synthesis parameters: *A. indica* leaf amount, plant extract-to-$AgNO_3$ ratio (reactant ratio), and incubation time were optimized. Physicochemical characterization of the optimized AgNPs was carried out using various analytical techniques, including ultraviolet–visible light (UV–Vis) spectroscopy, field emission scanning electron microscopy (FESEM), energy dispersive X-ray (EDX) spectroscopy, transmission electron microscopy (TEM), dynamic light scattering (DLS), and powder X-ray diffraction (XRD). Subsequently, the *in vitro* fungicidal effect of the green AgNPs against *Fusarium* isolates collected from the soils of disease-prone districts in Bangladesh was evaluated. Their effects on seed surface disinfection, germination, and their potential to cure and manage Bakanae disease under net-house conditions were also investigated.

2. Materials and methods

2.1. Collection and preparation of A. indica leaf extract

Fresh and healthy *A. indica* leaves were collected from Islamic University, Kushtia, Bangladesh, and washed thoroughly under running tap water, followed by double-distilled water (ddH_2O) to remove dirt. The cleaned leaves were air-dried at room temperature, finely chopped, and placed in Erlenmeyer flasks. Water (ddH_2O) was added to the flask, boiled at 100 °C for 20 min, cooled, filtered, and stored at 4 °C until nanoparticle synthesis (Fig. S1). A schematic representation of the optimization of green AgNPs from *Ai*LAE, characterization, and antifungal sensitivity tests is shown in Fig. S2.

2.2. Biosynthesis of A. indica leaf extract-mediated AgNPs

The green synthesis of AgNPs was performed according to a previously described protocol [10,17]. *Ai*LAE was mixed with silver nitrate ($AgNO_3$, Sigma-Aldrich, St. Louis, MO, USA) solution, followed by incubation at 85 °C in a hot air performance incubator (AP120, Froilabo, Meyzieu, France). The color change of the reaction mixture from colorless to yellow and finally to red-brown indicated the biosynthesis of AgNPs. All other chemicals were purchased from Sigma-Aldrich (St. Louis, MO, USA).

2.3. Optimization of synthesis parameters

Five different amounts of *A. indica* leaves (2, 5, 10, 15, and 20 g) and a wide range of reactant ratios and incubation times, ranging from 1:4 to 1:99 and 0.5–20 h, respectively, were explored for AgNP biosynthesis based on the literature [17–21] and after preliminary investigations. Determining the optimum amount of leaf, reactant ratio, and incubation time is very important for the biosynthesis of the desired AgNPs with improved physicochemical properties, that is, tiny, spherical, monodispersed, highly crystalline, and long-term stability. The temperature was kept constant at 85 °C during the optimization process based on a previous study [10] and after preliminary investigations. All experiments were performed in triplicates.

2.3.1. Amount of A. indica leaf and reactant ratio

The optimization process began with the formation of AgNPs from aqueous extracts of five different amounts of *A. indica* leaves. From each of the above extracts, 1 mL was mixed with different concentrations of $AgNO_3$ to prepare mixtures with ratios of 1:4, 1:9, 1:14, and 1:19 (final concentrations of 1 mM). After incubation at 85 °C for 1 h, the absorption spectra of the mixtures were measured as a function of reaction time using a UV–Vis spectrophotometer (U-2900 UV/VIS Spectrophotometer 200 V, HITACHI, Tokyo, Japan). To confirm the optimal amount of leaf extract and reactant ratio, AgNPs were biosynthesized using extracts from four different amounts (2, 5, 10, and 15 g, excluding 20 g) of leaves at different ratios of reactants, following the same procedure as above. Subsequently, the mixtures were incubated for different durations and their absorption spectra were measured. Based on these results, the optimal amount of leaf extract and reactant ratio were selected for further investigation.

2.3.2. Incubation time

Optimization of the incubation time was carried out based on color development and UV–Vis spectral analysis of the reaction mixtures (here, only the optimal amount of leaf and reactant ratio were used). After incubating the mixtures (maintaining the final volume and concentration at 100 mL and 1 mM, respectively) for different durations (0, 10, 20, 30, 40, 50, 60, 120, 180, 240, 300, and 360 min), the color changes and absorption spectra were monitored and recorded. The optimal incubation time was selected based on spectral analysis and used for subsequent experiments.

2.4. Estimation of concentration of optimized AgNPs

The concentration of the optimized AgNPs in the aqueous solution was estimated based on a calibration curve prepared from commercial AgNPs (65–75% Ag basis, product no. 85131). AgNPs were dispersed in sterile ddH_2O using an ultrasonicator (UC-40A; Biobase Industry Co. Ltd., Jinan, China). Subsequently, solutions at different concentrations of AgNPs (1.5–20.0 μg/mL) were prepared with sterile ddH_2O and taken into quartz cuvettes, followed by absorption measurement at 404 nm against a blank. A blank was prepared by replacing the AgNP solution with sterile ddH_2O.

2.5. Examination of stability of optimized AgNPs

The stability of optimized AgNPs in aqueous solution (kept in the dark at room temperature over for 18 months) was evaluated based on the analysis of the surface plasmon resonance (SPR; λ_{max} and peak width) band of UV–Vis spectra.

2.6. Physicochemical characterization of optimized green AgNPs

Optimized green AgNPs were separated and purified from the reaction mixtures by continuous centrifugation (16,658×*g*, 1610, Universal 32R, Hettich Zentrifugen, Tuttlingen, Germany) for 20 min at 4 °C with sterile ddH_2O [17]. The obtained pellets were washed repeatedly (3–4 times) with ddH_2O to ensure better separation of the AgNPs from other contaminants. After drying the pellets

at 60 °C in an oven (AP120, Froilabo, Meyzieu, France), the dried AgNPs were kept at 4 °C for further characterization.

The surface morphology, shape, and particle size distribution of the AgNPs were characterized using a FESEM device equipped with an EDX detector (JSM-7610F, JEOL Ltd., Akishima, Tokyo, Japan) operating at an acceleration voltage of 15 kV. The elemental distribution of the AgNPs was confirmed using EDX spectroscopy. The average particle size of the AgNPs was determined using a particle size analyzer (ZEN3600 Zetasizer, Malvern, Worcestershire, UK). The morphology, size, and shape of the AgNPs were determined using TEM image analysis. TEM (Talox F200X, Thermo Fisher Scientific, Hillsboro, OR, USA) image acquisition was performed under the following conditions: autofocus, microtrace, autodrive, live FFT display, auto pre-irradiation (API), 120 kV accelerated voltage, multiple lens configurations including a standard lens for unsurpassed high contrast, and a class-leading UHR lens for high resolution. A TEM grid was prepared by placing a drop of the bioreduced diluted solution on a carbon (C)-coated copper grid and drying it under a lamp.

The crystalline nature of green AgNPs was determined through the analysis of the XRD patterns of the powder AgNPs sample using an X-ray diffractometer (Philips PW 3040 X'Pert Pro, Eindhoven, Netherlands) using Cu Kα-radiation ($\lambda = 1.54$ Å), tube voltage of 33 kV, and tube current of 45 mA. The intensities were measured at 2θ values ranging from 10° to 90° at a continuous scan rate of 10°/min.

2.7. Collection, preservation, and molecular identification of fungal isolates

Soil fungal isolates were collected from three bakanae-prone districts (Habiganj, Cumilla, and Gazipur) by the Plant Pathology Division of Bangladesh Rice Research Institute (BRRI), Gazipur, Bangladesh, and named fungal isolates (40), (58), and (65), respectively, for convenience. The isolates were preserved on potato dextrose agar (PDA; Merck, Darmstadt, Germany) plates containing 4 g/L potato extract, 20 g/L glucose, and 15 g/L agar at 4 °C.

All three isolates were identified using PCR. Genomic DNA was extracted from the isolates for molecular characterization. To this end, 2 mL of a 24–36 h fresh culture of each isolate was centrifuged (Sorvall Legend Micro 17R centrifuge, Thermo Scientific, Waltham, MA, USA) at 13,845×*g* at room temperature for 10 min, and the supernatant was discarded. Nuclease-free water (500 μL) was added, followed by centrifugation at 13,845×*g* for 10 min, and this step was repeated twice. The supernatant was discarded, and the pellet was crushed in CTAB buffer (300 μL) using a crushing ball. Phenol:chloroform:isoamyl alcohol (25:24:1, v/v/v) was added, mixed gently by inversion, and maintained at room temperature for 10 min before centrifuging the sample at 13,845×*g* for 10 min. The aqueous upper layer (~200 μL) was transferred to a fresh tube containing an equal volume of isopropyl alcohol, mixed well, and kept for 10 min at room temperature. Subsequently, the samples were centrifuged at 13,845×*g* for 10 min, followed by supernatant removal and cold ethanol (70%, 700 μL) addition without disturbing the pellet. Finally, after centrifugation at 13,845×*g* for 5 min, the supernatant was decanted, the pellet was air-dried, and the dried pellet was re-suspended in TE buffer and stored at −20 °C for further analysis.

To amplify the target gene sequences, PCR reaction (reaction volume of 20 μL containing 10 μL of master mix (Thermo Fisher Scientific, Waltham, MA, USA), nuclease-free water (New England Biolabs, Ipswich, MA, USA) 4 μL, and primer (IDT, Singapore Science Park II, Republic of Singapore) forward and reverse 0.5 μL each (ITS1/4-F: 5′-GAAGTAAAAGTCGTAACAAG-3′) and ITS1/4-R: 5′-CCTCCGCTTATTGATATGC-3′) was performed by taking 5 μL of extracted genomic DNA in a Thermal Cycler (WD-9402B, BioBase, Jinan, China). The PCR condition was as follows: initial denaturation at 94 °C for 5 min, followed by 35 cycles of denaturation at 94 °C for 30 s, annealing at 53 °C for 30 s, extension at 72 °C for 1 min, and a final extension at 72 °C for 7 min.

2.8. In vitro antifungal activity determination of green AgNPs

2.8.1. Preparation of inoculum

Fungal isolates (40, 58, and 65) were cultured on PDA plates and incubated for 7–14 days at 28 ± 2 °C. Small pieces of agar containing the fungus were cut from the peripheral region of the plate using a scalpel and transferred to another plate for radial growth. A 14-day-old culture of each isolate was used as an inoculum.

2.8.2. Antifungal activity evaluation

The antifungal potential of *Ai*LAE and optimized green *Ai*LAE-AgNPs was determined using a food poisoning technique [22]. Colloidal solutions of AgNPs at 17.24 μg/mL were mixed with PDA solutions to prepare mixtures with final concentrations of 1.724, 3.448, 5.172, 6.89, 8.62, 10.34, and 12.07 μg/mL. The mixtures were subsequently poured into Petri dishes (90 mm diameter) to prepare the experimental plates. Another plate was prepared by mixing 1 mL *Ai*LAE (the concentration used for AgNPs synthesis) with PDA solution (when cooled to around 55 °C) following the same procedure. A control PDA plate was prepared without AgNPs. The 14-day-old fungal cultures were cut with a scalpel and placed at the center of each Petri dish. Subsequently, all plates were incubated at 28 ± 2 °C for 7–14 days in an incubator (Cool Incubator 23, Domel, Železniki, Slovenia) until the positive control plate was completely covered with fungal mycelia. Each treatment was replicated three times in a Complete Randomized Design (CRD) in the laboratory. The percentage mycelial growth inhibition in the control and experimental plates was measured and calculated using Eq. (1):

$$I = (R_c - R_i) \ / \ R_c \times 100 \quad (1)$$

where R_c and R_i are mycelial growth in the control and experimental plates (mm), respectively, and I is the inhibition of mycelial growth. Furthermore, the concentrations sufficient to effectively inhibit 50% mycelial growth (EC_{50}) for all fungal isolates were estimated using a previously described method [23].

2.9. Effect of optimized green AgNPs on seed surface disinfection, germination, and management of bakanae in net-house condition

2.9.1. Disinfection of Fusarium-infested seeds surfaces with AgNPs

Conidia from 2-week-old subcultures of all *Fusarium* isolates (40, 58, and 65) were scraped from PDA plates into separate test tubes, 25 mL sterile ddH_2O was added, and the tubes were vortexed. One milliliter of each conidial suspension was serially diluted, spread on PDA, and incubated at 28 ± 2 °C for 3 days, followed by enumeration. The CFU counts of each isolate (40, 58, and 65) were 3.3×10^6, 8.2×10^6, and 9.5×10^6, respectively, and adjusted to a final concentration of 1×10^6 conidia/mL with ddH_2O. Rice (F1 Hybrid, China, is a highly susceptible cultivar to *Fusarium* species) seeds (200/100 mL ddH_2O) were submerged in a 250 mL Erlenmeyer flask for 10 min and vortexed for 3 min. This process was repeated three times to clean the seeds. Afterward, the seeds were air-dried on a clean bench for 1 h. Dried seeds were soaked in the final individual conidial suspension at 25 ± 2 °C for 24 h to facilitate their attachment to the seed surface. The fungi-infested seeds were further air-dried on a clean bench for 1 h. Forty infested seeds of each isolate were completely flooded in 100 mL Erlenmeyer flasks containing 17.24 μg/mL of AgNPs. In parallel, 40 infested seeds from each isolate were plunged into sterile ddH_2O as a positive control. To measure the initial CFU in untreated seeds, five seeds of each isolate were placed in sterile microcentrifuge tubes containing 1 mL of sterile ddH_2O and centrifuged in a microcentrifuge machine at 216×*g* for 3 min. The same procedure was followed for the treated seeds; however, five seeds of each isolate were collected after exposure for 1, 3, 6, 12, and 24 h. After centrifugation, 100 μL conidia solution of the treated and non-treated seeds of each isolate was taken, serially diluted with sterile ddH_2O, spread on PDA, and incubated at 25 ± 2 °C for 3 days, followed by enumeration. The experiment was repeated thrice.

2.9.2. Seed germination test and management of bakanae in net-house condition

The seed germination test was performed in Petri dishes (90 mm) as follows: the infested-seeds were treated with AgNPs at a concentration of 17.24 μg/mL for 24 h, and subsequently, air-dried on sterile filter paper. Finally, all Petri dishes containing the 10 treated seeds were incubated in the dark and allowed to germinate under ambient conditions.

The trial for bakanae disease management in the net-house condition was carried out in rectangular-sized stainless steel trays (21″ length × 17″ width) on the roof of the faculty building of the Biological Sciences of Islamic University. Seeds were germinated on soils collected from the bakanae-prone districts of Habiganj, Cumilla, and Gazipur. A total of 27 trays were equally divided into three groups, and each group contained nine trays (three trays per isolate): (i) positive control, in which seeds were soaked in ddH_2O, air-dried, and sown on soil without any fungal infestation or AgNP treatment; (ii) negative control, in which seeds were infested with each fungal isolate without AgNP treatment; and (iii) experimental, in which seeds were both fungi-infested and AgNP-treated. Each tray contained 20 seeds sown in 5″ apart, with an inter-plant distance of 4″. Seeds were infested with individual fungal isolates following the procedures described in section 2.9.1. The experimental group was treated with AgNPs at a dose of 17.24 μg/mL at 10-day intervals for 40 days. Each experiment was repeated three times and each concentration included three replicates.

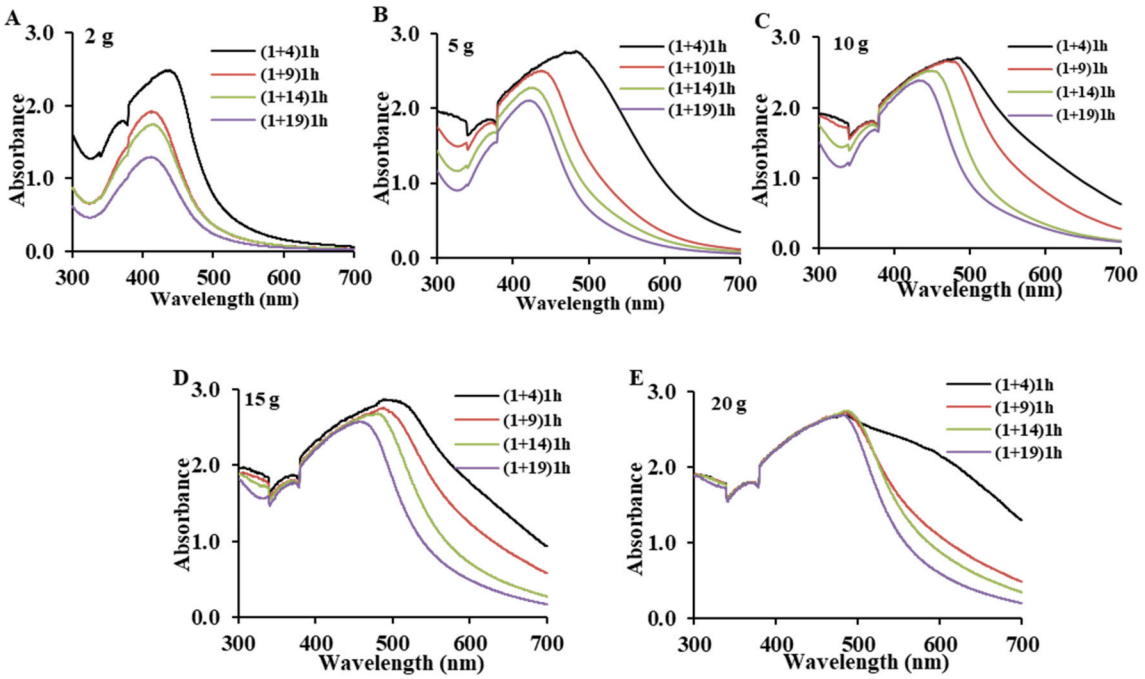

Fig. 1. UV–Vis spectra of AgNPs using (**A**) 2 g, (**B**) 5 g, (**C**) 10 g, (**D**) 15 g, and (**E**) 20 of *Azadirachta indica* leaf at leaf extract-to-$AgNO_3$ solution ratios of 1:4, 1:9, 1:14, and 1:19 (v/v) incubated at 85 °C for 1 h.

3. Results and discussion

3.1. Primary confirmation of AgNPs biosynthesis based on color change

Green AgNPs were produced through the reduction of Ag^{+} ions by *Ai*LAE, as observed primarily by the color change of the reaction solution (Fig. S3). The colloidal red-brown color change was due to the excitation of surface plasmon vibrations in the metal nanoparticles [24]. Similar changes in color due to the reaction between *Ai*LAE and $AgNO_3$ have been previously reported [17]; therefore, the complete reduction of Ag^{+} ions was confirmed. The functional groups present in the bioactive compounds of *Ai*LAE, particularly flavanones, terpenoids, and alkaloids, play the most important roles in capping, stabilizing, and reducing Ag^{+} to Ag^{0} [10]. Subsequently, Ag nuclei are formed owing to the further reduction of Ag^{+}, and the nucleation of such nuclei results in the synthesis of AgNPs [4].

3.2. Optimization of synthesis parameters

3.2.1. Amount of A. indica leaf and reactant ratio

The UV–Vis spectra of AgNPs obtained from the extracts of different amounts of *A. indica* leaves (2, 5, 10, 15, and 20 g), keeping other variables constant, are shown in Fig. 1A–E. UV–Vis spectroscopy can be used to confirm the formation and stability of AgNPs in aqueous solutions, and the size and shape of the AgNPs can be roughly determined from the peak position and shape or width of the absorption band (SPR band). Only a single SPR band is expected in the absorption spectra of spherical nanoparticles, whereas anisotropic particles can produce two or more SPR bands depending on the shape of the particles [25]. As shown in Fig. 1A–E, the spectrum of the 1:19 ratio of 2 g of leaf extract exhibited a single SPR band, suggesting that the AgNPs were spherical. However, except for the one above, all spectra from all extracts at all ratios were anisotropic because they gave rise to two or more SPR bands, indicating variation in the shapes of the biosynthesized AgNPs.

Fig. 2 shows the UV–Vis spectra of the AgNPs produced using 2 g of *A. indica* leaves and different ratios (v/v) of the extract-to-$AgNO_3$ solution at different time intervals. The 1:9 reactant ratio clearly exhibited an anisotropic curve (Fig. 2A), and the same phenomenon was observed for the 1:14 ratio over time (Fig. 2B). Conversely, single-SPR flat curves were initially observed after 30 and 60 min of incubation at a 1:19 ratio (Fig. 2C). However, with increasing reaction time (up to 4 h), the curves became sharper and the SPR bands became narrower, and the peaks shifted toward shorter wavelengths, indicating the formation of monodisperse and small-sized AgNPs. As the reaction time increased, the absorbance intensity of the reaction mixture increased, indicating enhanced formation of AgNPs. A similar observation has been reported previously [17]. The absorption maximum was recorded as 0.760 at 408.5 nm wavelength, 0.948 at 407.5 nm, 1.235 at 403.5 nm, 1.431 at 403 nm, and 1.498 at 407 nm for 30 min, 1 h, 2 h, 4 h, and 8 h of reaction, respectively. AgNPs usually exhibit an SPR band due to free electron excitation in the visible range of 390–500 nm, as determined by

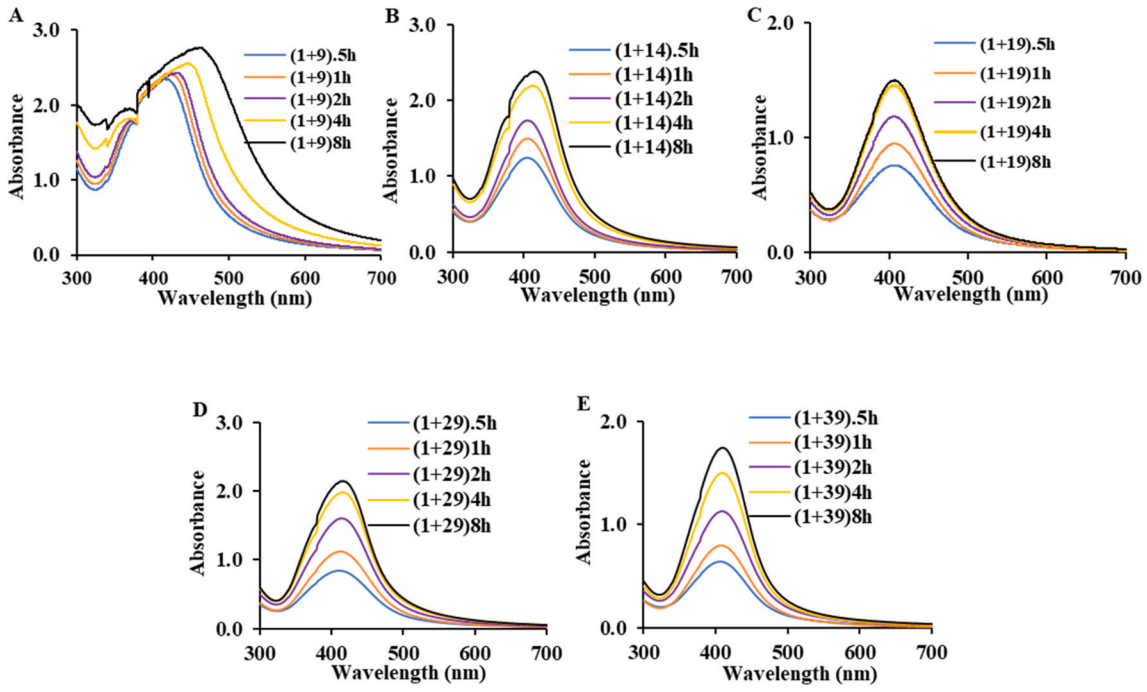

Fig. 2. UV–Vis spectra of AgNPs formed from 2 g *Azadirachta indica* leaf extract and $AgNO_3$ solution at the ratios of (**A**) 1:9, (**B**) 1:14; (**C**) 1:19; (**D**) 1:29; and (**E**) 1:39 (v/v) incubated at 85 °C for 0.5, 1, 2, 4, and 8 h, respectively.

UV–Vis absorption spectroscopy [26]. In all cases, absorption bands were observed within this range, confirming the formation of AgNPs. Moreover, AgNPs generated by incubation for 2 and 4 h showed that the intensity of the SPR band increased without any shift in the peak wavelength. However, the band shifted toward red and an anisotropic curve was observed upon further increasing the reaction time (8 h), suggesting that incubation between 2 and 4 h may be the optimal time for the formation of monodisperse and small-sized AgNPs. It was also observed that the formed AgNPs exhibited two or more SPR bands with increasing reaction time (Fig. 2B–D, and E). Furthermore, the curves of the 1:29 (Fig. 2D) and 1:39 (Fig. 2E) ratios were flatter and shifted toward red, suggesting larger AgNPs compared to the 1:19 ratio (Fig. 2C). Therefore, a ratio (1:19) was observed to be the optimal reactant ratio for the production of the desired AgNPs. This result is consistent with that of a previous study that reported that the biosynthesis of optimal AgNPs occurs at a specific plant extract-to-$AgNO_3$ ratio [27].

Again, the AgNPs produced from 5 g of the leaf extract at all ratios exhibited anisotropic curves at different reaction times (Fig. 3). This may be due to the presence of a higher concentration of phytochemicals, which accelerated the reducing power and the formation of two or more flat curves. Figs. 4 and 5 show that all the spectra of the biosynthesized AgNPs from 10 to 15 g of *Ai*LAE were anisotropic and that the curves were flatter and shifted toward red with increasing time, suggesting an increase in particle size due to diffusion growth, aggregation, or a combination. Therefore, if *Ai*LAE is used at concentrations above a certain threshold value, it is not suitable for AgNP formation [21]. In this study, the optimal conditions for the formation of monodisperse, spherical, and small-sized AgNPs were 2 g *Ai*LAE at a 1:19 reactant ratio and an incubation time between 2 and 4 h.

3.2.2. Incubation time

The color development of the reaction mixture containing 2 g *Ai*LAE and a reactant ratio of 1:19 at different time intervals is presented in Fig. 6A. The first two Erlenmeyer flasks on the left side of the figure indicate the *Ai*LAE and $AgNO_3$ solutions, respectively. At 0 min, no color change was noted; however, a yellow color appeared at 20 min, which deepened to reddish-brown and finally to dark red as the incubation time increased. Therefore, the color intensity increased with incubation time [17]. Interestingly, after 180 min of incubation, almost no color change was observed in the reaction mixture, indicating complete bio-reduction of Ag^{+} to Ag^{0}. Subsequently, UV–Vis spectroscopic absorption measurements of each reaction mixture were carried out at each time interval. The absorption maximum was recorded as 0.291 at 419 nm wavelength, 0.485 at 417 nm, 0.698 at 412 nm, 0.801 at 411 nm, 0.911 at 410.5 nm, 1.049 at 410 nm, 1.185 at 407 nm, 1.455 at 405.5 nm, 1.593 at 404 nm, 1.663 at 413.5 nm, and 1.724 at 421 nm for 0, 10, 20, 30, 40, 50, 60, 120, 180, 240, 300, and 360 min of reaction, respectively (Fig. 6B). It can be seen that the intensity of the SPR band increased with increasing incubation time, and the SPR band shifted toward blue up to the incubation time of 240 min (4 h). However, further increasing the reaction time (>240 min) resulted in a band shift toward red, suggesting that incubation of the reaction mixture for 4 h was the optimal time for the formation of monodisperse, small-sized AgNPs. Moreover, the maximum absorption peak observed at 404 nm after 240 min of incubation indicated a size of approximately 20 nm [28]. Therefore, it has been confirmed from the above discussions that the condition for producing optimized AgNPs (monodisperse, spherical, and small-sized) in this study is the 2g *Ai*LAE

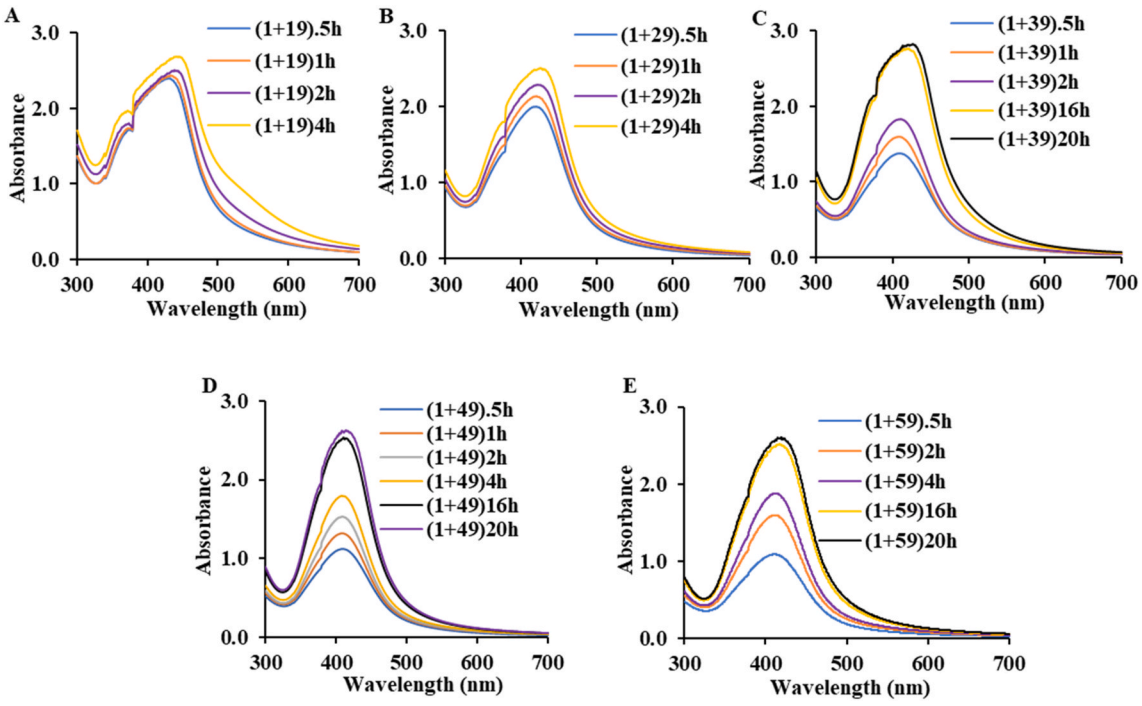

Fig. 3. UV–Vis spectra of AgNPs formed from 5 g *Azadirachta indica* leaf extract and $AgNO_3$ solution at the ratios of (**A**) 1:19, (**B**) 1:29, (**C**) 1:39, (**D**) 1:49, and (**E**) 1:59 (v/v) incubated at 85 °C for different durations.

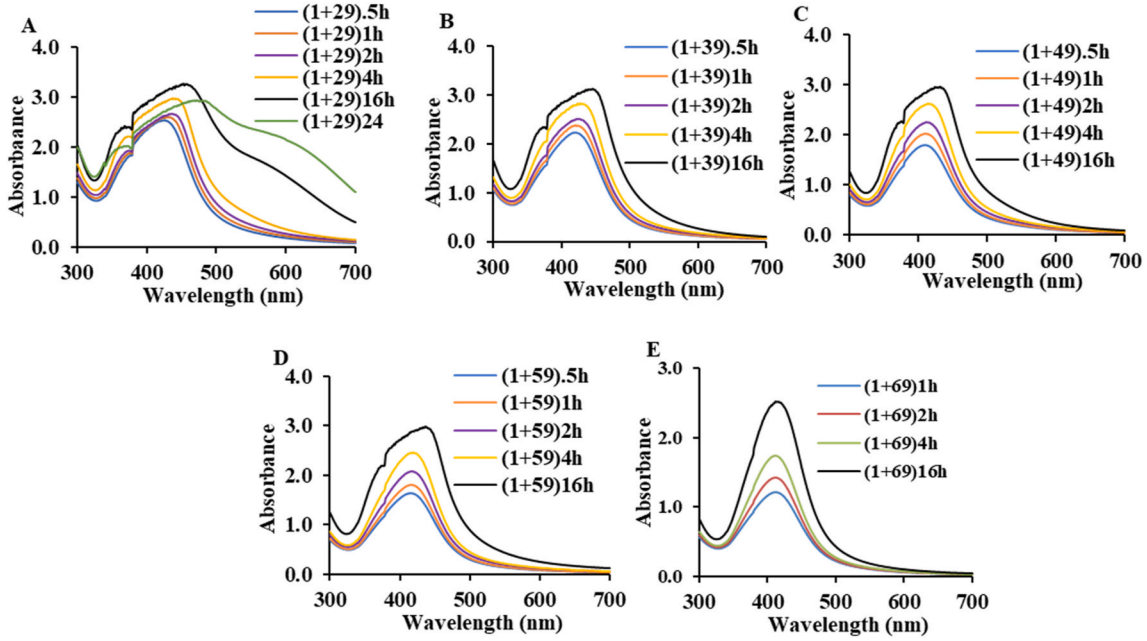

Fig. 4. UV–Vis spectra of AgNPs formed from 10 g *Azadirachta indica* leaf extract and $AgNO_3$ solution at the ratios of (**A**) 1:29, (**B**) 1:39, (**C**) 1:49, (**D**) 1:59, and (**E**) 1:69 (v/v) incubated at 85 °C for 0.5, 1, 2, 4, and 16 h, respectively.

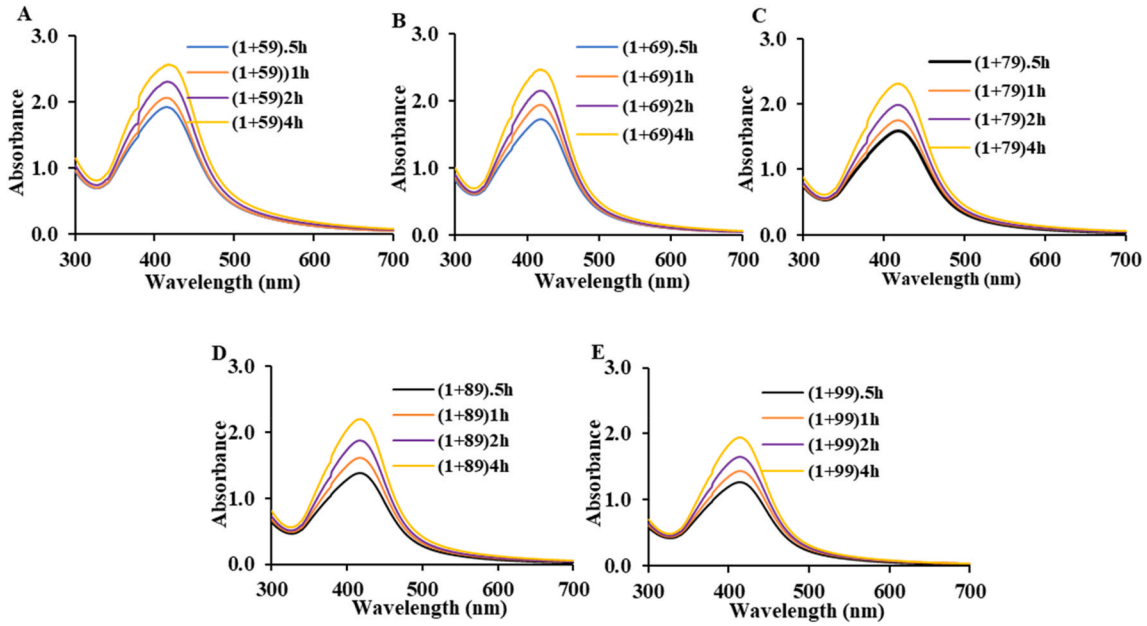

Fig. 5. UV–Vis spectra of AgNPs formed from 15 g *Azadirachta indica* leaf extract and $AgNO_3$ solution at the ratios of (**A**) 1:59, (**B**) 1:69; (**C**) 1:79; (**D**) 1:89; and (**E**) 1:99 (v/v) incubated at 85 °C for 0.5, 1, 2, and 4 h, respectively.

in a 1:19 reactant ratio incubated for 4 h at 85 °C.

3.3. Estimation of concentration of optimized green AgNPs

The concentration of the optimized green AgNPs was estimated based on the calibration curve of the standard AgNP solutions ($y = 0.0991x + 0.027$, $R^2 = 0.9975$). The absorbance of standard AgNP solutions increased with increasing AgNP concentration (Fig. 6C). Similar observations have been reported previously [29]. The high R^2 value shows that the standard curve can be applied to reliably

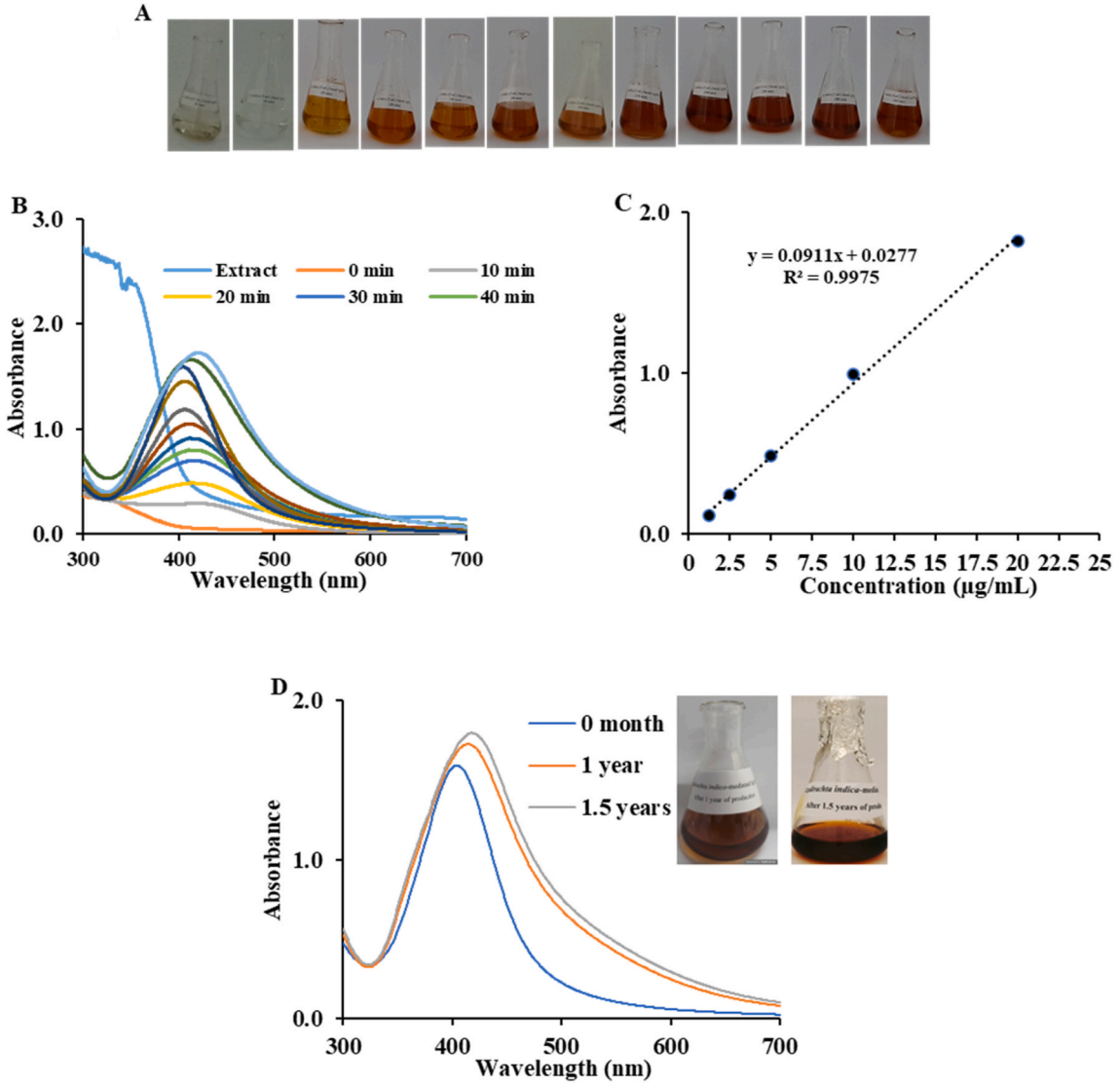

Fig. 6. (**A**) Color progression of colloidal AgNPs solution biosynthesized from 2 g *Azadirachta indica* leaf extract in a 1:19 ratio (v/v) incubated at 85 °C. The first two Erlenmeyer flasks on the left side of the figure indicate the *Ai*LAE and $AgNO_3$ solutions, respectively. The subsequent flasks represent the mixtures incubated for 0, 10, 20, 30, 40, 50, 60, 120, 180, 240, 300, and 360 min, respectively; (**B**) UV–Vis spectra of the reaction mixtures at each incubation time point; (**C**) Calibration curve of standard commercial AgNPs; (**D**) Stability test of optimized green AgNPs over for 18 months based on (SPR; λ_{max} and peak width) band of UV–Vis spectra.

estimate the concentration of optimized AgNPs (17.24 µg/mL, maximum absorption 1.593 at 404 nm).

3.4. Stability test of AgNPs

As can be seen from Fig. 6D, the maximum absorption of the optimized AgNPs was 1.593 at 404 nm, 1.727 at 415.5 nm, and 1.801 at 417.5 nm at 0 days (initial), 12 months, and 18 months, respectively. This indicates that the SPR band shifted slightly toward red owing to particle agglomeration during the storage of the aqueous solution. However, a sharp and high-amplitude peak similar to that in the spectrum at day 0 was observed; therefore, the optimized green AgNPs showed excellent stability even after 18 months. This high long-term storage ability may be due to the attachment of a large quantity of strong capping agents (flavanones, terpenoids, and alkaloids) to the surface of tiny AgNPs by preventing agglomeration [30]. In contrast, the maximum stability of *Ai*LAE-AgNPs was previously reported to be up to 4 months [31].

3.5. Physicochemical characterizations of optimized green AgNPs

3.5.1. DLS analysis

The particle size distribution of the AgNPs, as determined by DLS, is shown in Fig. 7A. The *Z*-average diameter value and polydispersity index (PDI) were found to be 49.96 nm and 0.271, respectively. The PDI value of a colloidal AgNPs solution less than 0.3 in addition to a single SPR band the monodisperse nanoparticles [32]. Our results are consistent with those in the literature and thus indicate the formation of small and monodisperse AgNPs.

3.5.2. FESEM-EDX analysis

The formation of green AgNPs can be discerned from FESEM analysis (Fig. 7B). The AgNPs were spherical, which is in agreement with the SPR peaks of the absorption spectra. The particles were also monodisperse with a narrow size distribution ranging from 30 to 50 nm. Some particles were larger than those inferred from the optical absorption spectra, owing to the agglomeration of nanoparticles, as the samples used to examine the morphology were maintained for a relatively longer time.

The chemical composition and purity of the AgNPs were investigated using the EDX spectra shown in Fig. 7C. The EDX spectrum exhibits a strong signal at 3 keV, which is the typical absorption peak for metallic AgNPs due to SPR [33], thus confirming the complete reduction of Ag compounds to AgNPs. However, two weak signals characteristic of C and oxygen (O) were also observed in the spectra within the range of 0–0.5 keV, which indicated the role of the phytochemicals present in *Ai*LAE as stabilizing/reducing agents. The absence of other elements in the spectra confirmed the purity of the green nanoparticles. The EDX analysis showed that the relative compositions of the elements were C 5.61%, O 4.48%, and Ag 89.92%. Thus, Ag was the main component of the particles, whereas the other elements served as capping organic agents bound to the surface of the AgNPs.

3.5.3. TEM analysis

Transmission electron microscopy (TEM) is the most efficient, preferred, and widely used method for directly measuring the size, size distribution, and morphology of nanoparticles because it provides high-resolution images of single nanoparticles in addition to analyzing their morphological properties [34]. Fig. 7D shows the morphological shape and size of the AgNPs obtained by TEM. The

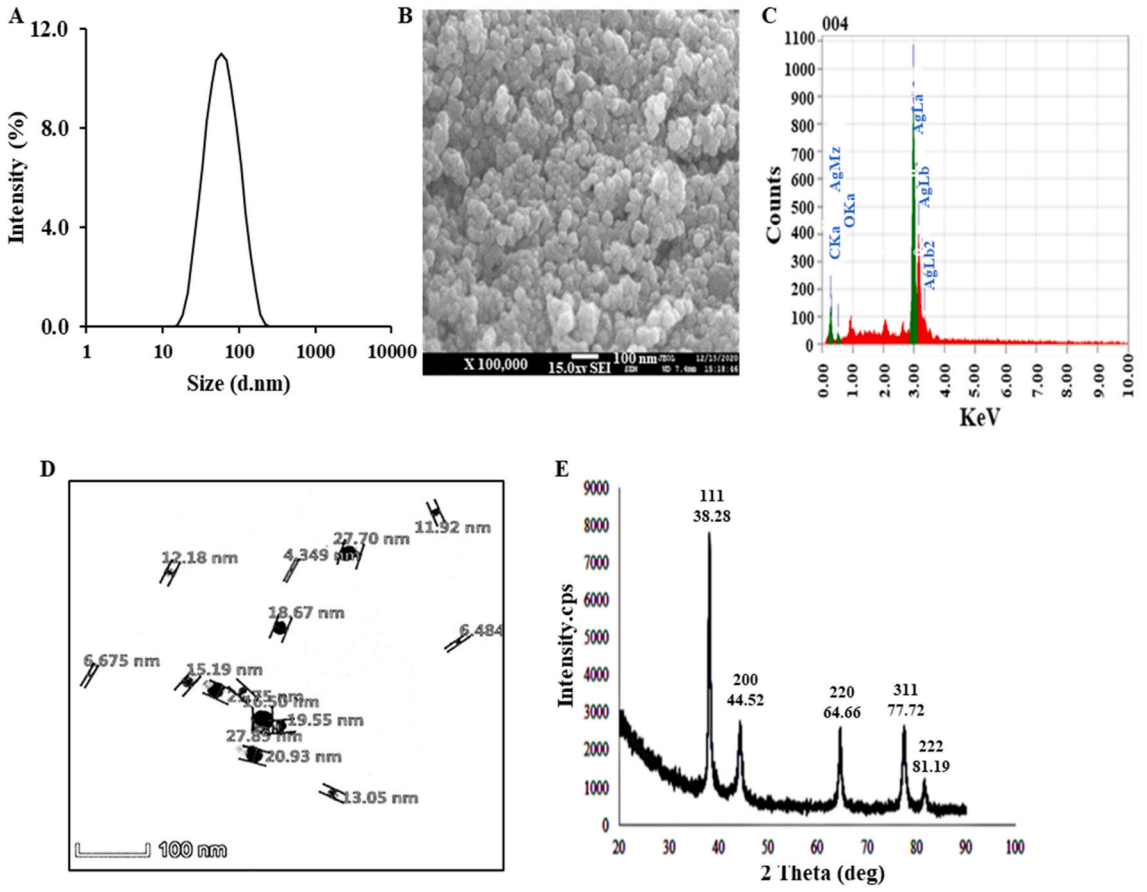

Fig. 7. (**A**) Size distribution by intensity using a particle size analyzer; (**B**) FESEM image; (**C**) Elemental analysis by EDX; (**D**) TEM image; and (**E**) XRD of optimized green AgNPs.

figure demonstrates that most of the particles are spherical, and the size of the particles ranges between 4 and 27 nm, which supports the size predicted from the UV–Vis spectrum. Moreover, the average diameter of the AgNPs observed by TEM was 15 nm, which is consistent with a previous study that reported an average size of 20 nm [10]. On the contrary, the average sizes of chemically synthesized AgNPs and their TATC conjugates were reported to be 24.83 ± 7.23 and 45.48 ± 5.13 nm [35], therefore, much larger than the average size of the present study.

3.5.4. XRD analysis

Fig. 7E shows the XRD pattern of the AgNPs. This was used to confirm that the biosynthesized particles were Ag and to determine their structure. The crystalline nature was confirmed by comparing the XRD patterns of the AgNPs, which exhibited sharp and clear peaks, with Bragg's diffraction patterns available in the Joint Committee on Powder Diffraction Standards (JCPDS) files. The XRD patterns of the AgNPs showed five main characteristic diffraction peaks for Ag at 2θ = 38.28°, 44.52°, 64.66°, 77.72°, and 81.9°,

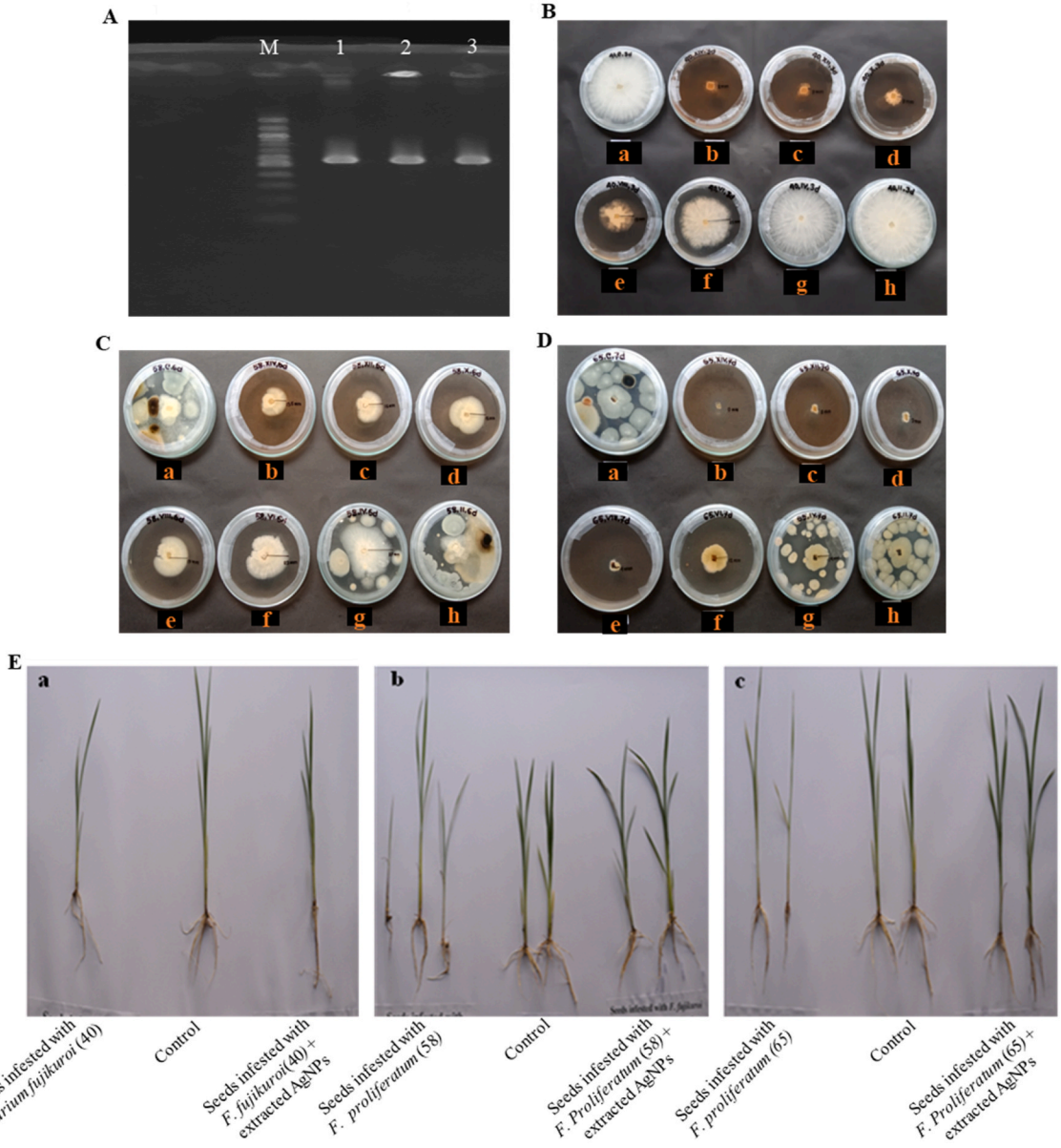

Fig. 8. (**A**) PCR amplification of *Fusarium* isolates (1 = 40, 2 = 58, 3 = 65; 100 bp ladder was used); Antifungal potential of AgNPs against (**B**) *Fusarium fujikuroi* (40) (**C**) *F. proliferatum* (58); (**D**) *F. proliferatum* (65) mycelial growth on PDA at different concentrations: **a** Control; **b-h** (12.08, 10.34, 8.62, 6.89, 5.172, 3.448, and 1.724 μg/mL, respectively) after 3 days of incubation at 28 ± 2 °C; and (**E**) *Fusarium* strain-infected rice plants (left), control (middle), and *Fusarium* strain-infected rice plants treated with green AgNPs (17.24 μg/mL) in net-house conditions (right): **a** *F. fujikuroi* (40); **b** *F. proliferatum* (58); and **c** *F. proliferatum* (65), respectively.

corresponding to the (111), (200), (220), (311), and (222) planes, respectively, which were indexed to the face-centered cubic (FCC) structure of metallic Ag. These peaks were analogous to those reported by Raj et al. [36] of $2\theta = 38.15^{\circ}$, 44.34°, 64.50°, 77.45°, 81.60°, and indicated the presence of phytochemical compounds in the *Ai*LAE. The strongest peak (111) at $2\theta = 38.20^{\circ}$ probably corresponds to the spherical nanoparticles crystallized in the FCC structure. Moreover, the (111) peak of the FCC materials exhibits the highest intensity, reflecting a high degree of AgNP crystallinity [33]. These results were in agreement with those obtained using DLS, FESEM, and XRD.

3.6. Molecular identification of Fusarium isolates

A representative image showing the PCR amplification of the target gene (*IST1/4*) of the three isolates separated by electrophoresis on a 1.5% agarose gel in 1X TAE buffer at 90 V is presented in Fig. 8A. Sequence analysis was performed using MiSeq Illumina (Macrogen Inc., Seoul, Republic of Korea), and similarities were identified using NCBI BLAST analysis (Table 1). The isolates (40, 58, and 65) were identified as *F. fujikuroi*, *F. proliferatum*, and *F. proliferatum*, respectively. It has been reported that the ribosomal internal transcribed spacer (ITS) is used as a DNA barcoding marker to identify the interspecies fungal variation [37]. Interestingly, our molecular findings demonstrate the presence of three different fungal strains.

3.7. Antifungal activity of green AgNPs

The antifungal potential of the optimized green *Ai*LAE-AgNPs against *Fusarium* strains is shown in Fig. 8B–D and Table 2. In the present study, *Ai*LAE alone did not inhibit mycelial growth in *F. fujikuroi* (40), *F. proliferatum* (58), or *F. proliferatum* (65) (Fig. S4). The presence of low quantities of phytochemicals in dilute concentrations of the leaf extracts was not sufficient to elicit strong antifungal properties [4]. However, the mycelial growth inhibition of *F. proliferatum* (65), *F. fujikuroi* (40), and *F. proliferatum* (58) was observed to be 100, 95.56, and 70% against green AgNPs at a concentration of 12.08 μg/mL on PDA media. Therefore, it was confirmed that AgNPs capped with *Ai*LAE synergistically enhanced antifungal potency compared to the extract alone [4]. Moreover, *Ai*LAE-AgNPs at a concentration of 400 μg/mL reported a maximum of 89% mycelial growth inhibition against *Fusarium* species in a previous study [38]. In another study, complete mycelial growth inhibition (100%) was noticed at 25 μg/mL by TDTC-AgNPs [35]. This study also reported 10^6 times better antifungal activity of the conjugate against *F. fujikuroi* than that of chemically synthesized AgNPs alone. The results obtained in the present study indicate that the optimized AgNPs could completely inhibit fungal growth, even at a significantly lower dosage than the previously reported *Ai*LE-AgNPs and TDTC-AgNPs. The antifungal activity of AgNPs depends on various factors, such as concentration, size, shape, and exposure time [2,39]. In this study, AgNPs exhibited *in vitro* antifungal activity against all three *Fusarium* strains in a concentration-dependent manner (i.e., increasing the concentration of AgNPs resulted in increased mycelial growth inhibition). A similar concentration-dependent relationship between AgNPs and antifungal activity was previously reported [2, 35]. Moreover, the EC_{50} values of AgNPs in our study were shown to be 5.50, 5.40, and 2.95 μg/mL for *F. fujikuroi* (40) and *F. proliferatum* (58 and 65), respectively. In comparison, the EC_{50} values of TDTC, AgNPs alone, and TDTC-AgNPs were found to be 15, 28, and 13 μg/mL, respectively, by Sharma et al. (15). These data suggest that the TDTC-AgNP conjugates successfully reduced the EC_{50} value of AgNPs alone, which was one of the main aims of this study because of the toxicological apprehensions associated with high doses of AgNPs. However, the EC_{50} value of TDTC-AgNPs was still much higher than that of green AgNPs in the present study. Therefore, it is evident that the optimized green AgNPs are more potent than the chemically synthesized AgNPs and the TDTC-AgNP formulation.

The antifungal molecular mechanisms of AgNPs against wheat *Fusarium graminearum* (which causes Fusarium head blight), one of the most destructive phytopathogens, have recently been elucidated [40]. However, the exact molecular mode of action against *F. fujikuroi* and *F. proliferatum* has not yet been explored and is poorly understood, necessitating further studies. The underlying fungicidal mechanism of the developed AgNPs is hypothesized to primarily inhibit mycelial growth and conidial germination, which are linked to damage to cell wall and membrane integrity. After entry, they interact with internal cellular organelles or large biomolecules and generate high levels of ROS and free radicals, which cause dysfunction of metabolism, signal transduction, and genetic information processing, ultimately resulting in cell death [40].

Owing to their larger surface-to-volume ratio, smaller spherical AgNPs release more silver ions, which exert their higher antifungal potential [2,40]. The smaller the AgNPs, the faster they can cross cell walls and membranes. Subsequently, they interact with biological oxidizers to sustainably release silver ions, which bind strongly to intracellular organelles and biomolecules, and disrupt biological processes, resulting in cell death [2]. Nanoparticles of very small sizes (10–20 nm) can enter and exit the cell membrane more easily than larger nanoparticles [41]. In this study, the sizes of the green AgNPs ranged between 4 and 27 nm, with an average size of 15 nm, and hence exerted potent *in vitro* antifungal activity against three strains of *Fusarium* sp. In addition, AgNPs with a monodisperse size distribution, spherical shape, and high crystallinity have been reported to exhibit enhanced antifungal activity [2].

Table 1
Identification of *Fusarium* isolates using target gene amplification.

Sl. No.	Isolate	Location	Identification	Similarity (%)
1	40	Habiganj	*Fusariun fujikuroi*	99.82
2	58	Cumilla	*Fusariun proliferatum*	99.27
3	65	Gazipur	*Fusariun proliferatum*	100

Table 2
Concentration-dependent *in vitro* antifungal potential of green AgNPs against *Fusarium* strains.

Strains Name	Concentration of Green AgNPs (μg/mL)								
	12.08	10.34	8.62	6.89	5.17	3.45	1.72		EC_{50}
Fusarium fujikuroi (40)	95.56	93.33	88.89	71.11	44.44	00	00	Growth inhibition (%)	5.50
Fusarium proliferatum (58)	70.00	64.44	60.00	57.78	48.89	40.00	00		5.40
Fusarium proliferatum (65)	100.00	95.56	93.33	91.11	73.33	68.89	00		2.95

Here, optimized *Ai*LAE-AgNPs were found to be monodisperse, highly spherical, and crystalline in nature, and therefore exhibited enhanced antifungal activity.

Among the *Fusarium* species, although *F. fujikuroi* is the most virulent and common fungal pathogen, *F. proliferatum* is also responsible for Bakanae disease in rice [42]. Our results indicated that AgNPs were highly effective against *F. proliferatum* (65), followed by *F. fujikuroi* (40), and moderately effective against *F. proliferatum* (58). The *F. proliferatum* (58 and 65) strains probably had genetic divergence, which could explain their significant differences in sensitivity to AgNPs. Thus, the optimization process had a profound influence on the antifungal potential of AgNPs by improving their physicochemical characteristics.

3.8. Effect of optimized green AgNPs on seed disinfection, germination, and bakanae management in net-house condition

The CFU counts of *Fusarium* strains on the surfaces of rice seeds treated with the optimized green AgNPs at different time intervals are presented in Table 3. On the surface of non-treated seeds (positive control), the CFU counts of individual strains (40, 58, and 65) were 4.6, 4.5, and 5.2 ($\times 10^5$/mL), respectively. However, when fungal-infested seeds were treated with AgNPs (17.24 μg/mL) for 1 h, CFU reductions of 95, 96, and 100% were observed for *F. fujikuroi* (40), *F. proliferatum* (58), and *F. proliferatum* (65), respectively. When the exposure time was increased to 3 h, 100% CFU reduction in *F. fujikuroi* (40) and *F. proliferatum* (58) was observed, indicating that the efficacy of AgNPs was also dependent on the exposure time [39]. In comparison, Jo et al. (2015) reported a 96.2% CFU reduction of *G. fujikuroi* after 6 h exposure to chemically synthesized AgNPs at a significantly higher concentration of 150 μg/mL. Hence, the optimized green AgNPs exhibit excellent potential as seed disinfectants at significantly low concentrations.

When the seeds were exposed to green AgNPs for an even longer duration (24 h) in Petri dishes, they germinated successfully and no abnormal seedlings were observed. Therefore, the developed AgNPs are nontoxic to rice seeds. This nontoxic nature may be attributed to the attachment of a maximum quantity of biocompatible capping agents [30]. Moreover, green AgNPs can act as antifungal agents against the plant pathogen *Fusarium* in rice seeds with high efficacy and safety. Although tomato plants treated with chemically synthesized AgNPs showed a significant reduction in early blight disease [35], *Fusarium* strain-infected rice plants treated with green AgNPs (17.24 μg/mL) in net-house conditions were noticed to be fully cured from the disease and had the appearance as normal rice plants (Fig. 8E). AgNPs have been reported to display significant antibacterial effects under *in vitro* conditions at 100 μg/mL [35], which is higher than the permitted level established by the Environmental Protection Agency (EPA).

Plants produce various phytohormones, such as auxins, abscisic acid, cytokinins, gibberellins, and brassinosteroids, which regulate their normal functioning (growth, development, reproductive processes, longevity, and even death). GA_3 plays an important role in regulating stem elongation during the juvenile stage, seed germination and dormancy, flowering, leaf expansion, and leaf and fruit senescence [43]. FFSC, the main pathogen responsible for rice bakanae, also produce auxins, cytokinins, and gibberellin hormones. The abnormal production of GA_3 in bakanae is solely attributed to typical bakanae symptoms, such as abnormally elongated seedlings [1]. However, among the FFSC, *F. fujikuroi* and *F. proliferatum* could only produce GA_3 [42]. Both pathogens, in addition to GA_3 can also produce various secondary metabolites such as fumonisin (FUM), monilifornin (MON), fusaric acid (FA), indole acetic acid (IAA), and beauvericin (BEA) in infected plants attributing to the development of other symptoms. High production of FUM and FA has an opposite effect to that of GA_3, which is responsible for the stunted growth of seedlings [44]. Thus, it is evident that the optimized green AgNPs successfully regulated the abnormal production of GA_3, FUM, and FA by *F. fujikuroi* and *F. proliferatum* in infected rice plants (Fig. 8E). The mechanism of this regulation by AgNPs should be explored in future studies.

Thus, the above discussion provides strong evidence that the optimized *Ai*LAE-AgNPs have remarkable *in vitro* antifungal and seed disinfection activities against all *Fusarium* strains examined at significantly low concentrations. In addition, they did not show any adverse effects on germination, were stable for a long period (18 months) in aqueous form, and, most importantly, effectively managed rice bakanae under net-house conditions. Hence, they can be successfully applied under field conditions to control devastating diseases. However, latent adverse effects on plant health or genetic components, the smallest effective concentration in actual field conditions, cost-effectiveness, bakanae control mechanisms, effects on other phytopathogenic plant diseases, and long-term exposure effects on humans and animals need to be evaluated in future studies.

4. Conclusions

In conclusion, this report demonstrates a green, non-toxic, and effective approach for the management of rice bakanae disease-causing phytopathogens and *Fusarium* species under *in vitro* and net-house conditions, providing a significant improvement in sustainable agriculture. The approach explored the green synthesis of *Ai*LAE-AgNPs through the optimization of various reaction parameters, the effective concentration against the targeted phytopathogens (isolated from the soils of bakanae-prone areas), and subsequently, their successful application as nanofungicides in net-house conditions, The results showed that the optimized AgNPs

Table 3
Effect of optimized green AgNPs on the CFU reduction of *Fusarium* strain-infested seeds after different exposure durations (h; hour) and on germination.

Fusarium strains	*Fusarium* strains-infested seeds treated with AgNPs (17.24 μg/mL) after different exposure durations						
	1 h	3 h	6 h	12 h	24 h		Seed Germination (%)
F. fujikuroi (40)	95	100	100	100	100	CFU reduction of *Fusarium* strains (%)	100
F. proliferatum (58)	96	100	100	100	100		100
F. proliferatum (65)	100	100	100	100	100		100

were very small, uniform, spherical, highly crystalline, and long-term stable in aqueous solutions. AgNPs displayed mycelial growth inhibition and seed disinfection potential in concentration- and exposure time-dependent manners, respectively. Moreover, they exhibited remarkable inhibitory effects at significantly lower concentrations and shorter exposure times than chemically synthesized AgNPs reported in the literature. Most importantly, the optimized *Ai*LAE-AgNPs were non-toxic to seeds during germination and fully cured *Fusarium* sp.-infected rice plants under net-house conditions. The findings of this study underscore the high nano-fungicidal potency of optimized PEM-AgNPs as an effective alternative strategy for controlling phytopathogenic diseases while minimizing the negative ecological impacts associated with chemical fungicides. This study provides valuable insights into the expanding field of PEM-AgNPs as nanofungicides in agricultural systems and paves the way for further research and development in the pursuit of eco-friendly solutions for controlling plant diseases.

5. Data availability statement

Data included in article/supp. material/referenced in article.

CRediT authorship contribution statement

Quazi Shireen Akhter Jahan: Writing – review & editing, Investigation, Funding acquisition, Conceptualization. **Ziniya Sultana:** Investigation, Formal analysis. **Md. Asad Ud-Daula:** Writing – review & editing, Writing – original draft. **Md. Ashikuzzaman:** Investigation. **Md. Shamim Reja:** Investigation. **Md. Mahfuzur Rahman:** Investigation. **Amina Khaton:** Investigation. **Md. Abul Kashem Tang:** Conceptualization. **M. Safiur Rahman:** Investigation, Data curation. **Hossain Md. Faruquee:** Writing – review & editing, Formal analysis. **Seung Ju Lee:** Writing – review & editing. **A.T.M. Mijanur Rahman:** Writing – review & editing, Writing – original draft, Supervision, Investigation, Funding acquisition, Formal analysis, Data curation, Conceptualization.

Declaration of competing interest

The authors declare that they have no known competing financial interests or personal relationships that could have appeared to influence the work reported in this paper.

Acknowledgements

The authors wish to express their sincere thanks and appreciations to National Agricultural Technology Program-Phase II (NATP-2, Grants ID: 159), Sub-Project Completion Report (PBRG), the International Fund for Agricultural Development (IFAD), Rome, Italy, the International Development Association (IDA), and Ministry of Agriculture, Bangladesh for the research grant administered through the Bangladesh Agricultural Research Council (BARC), Dhaka, Bangladesh. The authors also grateful to Bangladesh Rice Research Institute (BRRI), Atomic Energy Commission, Dhaka, Bangladesh, and Islamic University, Kushtia, Bangladesh for providing research facilities.

Appendix A. Supplementary data

Supplementary data to this article can be found online at https://doi.org/10.1016/j.heliyon.2024.e27579.

References

[1] Y.N. An, C. Murugesan, H. Choi, K.D. Kim, S.-C. Chun, Current studies on bakanae disease in rice: host range, molecular identification, and disease management, MYCOBIOLOGY 51 (2023) 195–209, https://doi.org/10.1080/12298093.2023.2241247.
[2] H. Shi, H. Wen, S. Xie, Y. Li, Y. Chen, Z. Liu, N. Jiang, J. Qiu, X. Zhu, F. Lin, Y. Kou, Antifungal activity and mechanisms of AgNPs and their combination with azoxystrobin against *Magnaporthe oryzae*, Environ. Sci.: Nano 10 (2023) 2412–2426, https://doi.org/10.1039/D3EN00168G.
[3] S. Khan, M. Zahoor, R. Sher Khan, M. Ikram, N.U. Islam, The impact of silver nanoparticles on the growth of plants: the agriculture applications, Heliyon 9 (2023) e16928, https://doi.org/10.1016/j.heliyon.2023.e16928.

[4] D.H. Nguyen, T.N.N. Vo, N.T. Nguyen, Y.C. Ching, T.T. Hoang Thi, Comparison of biogenic silver nanoparticles formed by Momordica charantia and Psidium guajava leaf extract and antifungal evaluation, PLoS One 15 (2020) e0239360, https://doi.org/10.1371/journal.pone.0239360.

[5] A. Wasilewska, U. Klekotka, M. Zambrzycka, G. Zambrowski, I. Święcicka, B. Kalska-Szostko, Physico-chemical properties and antimicrobial activity of silver nanoparticles fabricated by green synthesis, Food Chem. 400 (2023) 133960, https://doi.org/10.1016/j.foodchem.2022.133960.

[6] S. Sharmin, M.B. Islam, B.K. Saha, F. Ahmed, B. Maitra, M.Z. Uddin Rasel, N. Quaisaar, M.A. Rabbi, Evaluation of antibacterial activity, in-vitro cytotoxicity and catalytic activity of biologically synthesized silver nanoparticles using leaf extracts of Leea macrophylla, Heliyon 9 (2023) e20810, https://doi.org/10.1016/j.heliyon.2023.e20810.

[7] S. Ali, X. Chen, M. Ajmal Shah, M. Ali, M. Zareef, M. Arslan, S. Ahmad, T. Jiao, H. Li, Q. Chen, The avenue of fruit wastes to worth for synthesis of silver and gold nanoparticles and their antimicrobial application against foodborne pathogens: a review, Food Chem. 359 (2021) 129912, https://doi.org/10.1016/j.foodchem.2021.129912.

[8] M. Ohiduzzaman, M.N.I. Khan, K.A. Khan, B. Paul, Biosynthesis of silver nanoparticles by banana pulp extract: characterizations, antibacterial activity, and bioelectricity generation, Heliyon 10 (2024) e25520, https://doi.org/10.1016/j.heliyon.2024.e25520.

[9] F. Zhan, X. Yan, F. Sheng, B. Li, Facile in situ synthesis of silver nanoparticles on tannic acid/zein electrospun membranes and their antibacterial, catalytic and antioxidant activities, Food Chem. 330 (2020) 127172, https://doi.org/10.1016/j.foodchem.2020.127172.

[10] M. Asimuddin, M.R. Shaik, S.F. Adil, M.R.H. Siddiqui, A. Alwarthan, K. Jamil, M. Khan, Azadirachta indica based biosynthesis of silver nanoparticles and evaluation of their antibacterial and cytotoxic effects, J. King Saud Univ. Sci. 32 (2020) 648–656, https://doi.org/10.1016/j.jksus.2018.09.014.

[11] S. Ganguli, S. Howlader, A.K.M.A. Ullah, F.R. Bhuiyan, A.A. Akhi, A. Hasan, K. Dey, S. Islam, F. Ali, A.K. Chakraborty, S. Bhattacharjee, B.K. Dey, Size controlled biosynthesis of silver nanoparticles using Ophiorrhiza mungos, Ophiorrhiza harrisiana and Ophiorrhiza rugosa aqueous leaf extract and their antimicrobial activity, Heliyon 9 (2023) e16072, https://doi.org/10.1016/j.heliyon.2023.e16072.

[12] M. Tariq, K.N. Mohammad, B. Ahmed, M.A. Siddiqui, J. Lee, biological synthesis of silver nanoparticles and prospects in plant disease management, Molecules 27 (2022) 4754, https://doi.org/10.3390/molecules27154754.

[13] M. Ansari, S. Ahmed, A. Abbasi, N.A. Hamad, H.M. Ali, M.T. Khan, I.U. Haq, Q. uz Zaman, Green synthesized silver nanoparticles: a novel approach for the enhanced growth and yield of tomato against early blight disease, Microorganisms 11 (2023) 886, https://doi.org/10.3390/microorganisms11040886.

[14] S. Adusei, S. Azupio, Neem: a novel biocide for pest and disease control of plants, J. Chem. 2022 (2022) 1–12, https://doi.org/10.1155/2022/6778554.

[15] M. Ahmed, D.A. Marrez, N. Mohamed Abdelmoeen, E. Abdelmoneem Mahmoud, M.A.-S. Ali, K. Decsi, Z. Tóth, Studying the antioxidant and the antimicrobial activities of leaf successive extracts compared to the green-chemically synthesized silver nanoparticles and the crude aqueous extract from Azadirachta indica, Processes 11 (2023) 1644, https://doi.org/10.3390/pr11061644.

[16] H. Wen, H. Shi, N. Jiang, J. Qiu, F. Lin, Y. Kou, Antifungal mechanisms of silver nanoparticles on mycotoxin producing rice false smut fungus, iScience 26 (2023) 105763, https://doi.org/10.1016/j.isci.2022.105763.

[17] Z. Sultana, S. Aktar, M.M. Rahman, A.S.M.A. Haque Akand, A. Ud Daula, M.A.K. Tang, D.K. Paul, B.S. Azhar, M.S. Raza, A.T.M.M. Rahman, Evaluation of the synergistic effect of Azadirachta indica-based silver nanoparticles in combination with antibiotics and hypoglycemic drugs: in vitro antimicrobial and in vivo antidiabetic activities, J. Sci. Technol. Res. 4 (2023) 91–100, https://doi.org/10.3329/jscitr.v4i1.67372.

[18] Y.L. Balachandran, S. Girija, R. Selvakumar, S. Tongpim, A.C. Gutleb, S. Suriyanarayanan, Differently environment stable bio-silver nanoparticles: study on their optical enhancing and antibacterial properties, PLoS One 8 (2013) e77043, https://doi.org/10.1371/journal.pone.0077043.

[19] S.A. Kumari, A.K. Patlolla, P. Madhusudhanachary, Biosynthesis of silver nanoparticles using Azadirachta indica and their antioxidant and anticancer effects in cell lines, Micromachines 13 (2022) 1416, https://doi.org/10.3390/mi13091416.

[20] P. Banerjee, M. Satapathy, A. Mukhopahayay, P. Das, Leaf extract mediated green synthesis of silver nanoparticles from widely available Indian plants: synthesis, characterization, antimicrobial property and toxicity analysis, Bioresour Bioprocess 1 (2014) 3, https://doi.org/10.1186/s40643-014-0003-y.

[21] P. Roy, B. Das, A. Mohanty, S. Mohapatra, Green synthesis of silver nanoparticles using Azadirachta indica leaf extract and its antimicrobial study, Appl. Nanosci. 7 (2017) 843–850, https://doi.org/10.1007/s13204-017-0621-8.

[22] F. Al-Otibi, S.A. Alfuzan, R.I. Alharbi, A.A. Al-Askar, R.M. Al-Otaibi, H.F. Al Subaie, N.M.S. Moubayed, Comparative study of antifungal activity of two preparations of green silver nanoparticles from Portulaca oleracea extract, Saudi J. Biol. Sci. 29 (2022) 2772–2781, https://doi.org/10.1016/j.sjbs.2021.12.056.

[23] L.A. Rivillas-Acevedo, M. Soriano-García, Isolation and biochemical characterization of an antifungal peptide from Amaranthus hypochondriacus seeds, J. Agric. Food Chem. 55 (2007) 10156–10161, https://doi.org/10.1021/jf072069x.

[24] S. Ahmed, Saifullah, M. Ahmad, B.L. Swam, S. Ikram, Green synthesis of silver nanoparticles using Azadirachta indica aqueous leaf extract, J Radiat Res Appl Sci 9 (2016) 1–7, https://doi.org/10.1016/j.jrras.2015.06.006.

[25] G. Mie, Beiträge zur Optik trüber Medien, speziell kolloidaler Metallösungen, Ann. Phys. 330 (1908) 377–445, https://doi.org/10.1002/andp.19083300302.

[26] S. Karimi, M. Mahdavi Shahri, Medical and cytotoxicity effects of green synthesized silver nanoparticles using *Achillea millefolium* extract on MOLT-4 lymphoblastic leukemia cell line, J. Med. Virol. 93 (2021) 3899–3906, https://doi.org/10.1002/jmv.26694.

[27] M. Ali, B. Kim, K.D. Belfield, D. Norman, M. Brennan, G.S. Ali, Green synthesis and characterization of silver nanoparticles using Artemisia absinthium aqueous extract — a comprehensive study, Mater. Sci. Eng. C 58 (2016) 359–365, https://doi.org/10.1016/j.msec.2015.08.045.

[28] D. Paramelle, A. Sadovoy, S. Gorelik, P. Free, J. Hobley, D.G. Fernig, A rapid method to estimate the concentration of citrate capped silver nanoparticles from UV-visible light spectra, Analyst 139 (2014) 4855, https://doi.org/10.1039/C4AN00978A.

[29] A. Bernabé-Antonio, A. Martínez-Ceja, A. Romero-Estrada, J.N. Sánchez-Carranza, M.C. Columba-Palomares, V. Rodríguez-López, J.C. Meza-Contreras, J. A. Silva-Guzmán, J.M. Gutiérrez-Hernández, Green synthesis of silver nanoparticles using Randia aculeata L. Cell culture extracts, characterization, and evaluation of antibacterial and antiproliferative activity, Nanomaterials 12 (2022) 4184, https://doi.org/10.3390/nano12234184.

[30] R. Javed, M. Zia, S. Naz, S.O. Aisida, N. ul Ain, Q. Ao, Role of capping agents in the application of nanoparticles in biomedicine and environmental remediation: recent trends and future prospects, J. Nanobiotechnol. 18 (2020) 172, https://doi.org/10.1186/s12951-020-00704-4.

[31] J. Hawadak, L.P. Kojom Foko, V. Pande, V. Singh, In vitro antiplasmodial activity, hemocompatibility and temporal stability of *Azadirachta indica* silver nanoparticles, Artif. Cells, Nanomed. Biotechnol. 50 (2022) 286–300, https://doi.org/10.1080/21691401.2022.2126979.

[32] R. Sadeghi, S.Gh Etemad, E. Keshavarzi, M. Haghshenasfard, Investigation of alumina nanofluid stability by UV–vis spectrum, Microfluid. Nanofluidics 18 (2015) 1023–1030, https://doi.org/10.1007/s10404-014-1491-y.

[33] M. Alam, Analyses of biosynthesized silver nanoparticles produced from strawberry fruit pomace extracts in terms of biocompatibility, cytotoxicity, antioxidant ability, photodegradation, and in-silico studies, J. King Saud Univ. Sci. 34 (2022) 102327, https://doi.org/10.1016/j.jksus.2022.102327.

[34] B. Lee, S. Yoon, J.W. Lee, Y. Kim, J. Chang, J. Yun, J.C. Ro, J.-S. Lee, J.H. Lee, Statistical characterization of the morphologies of nanoparticles through machine learning based electron microscopy image analysis, ACS Nano 14 (2020) 17125–17133, https://doi.org/10.1021/acsnano.0c06809.

[35] A.B. Sharma, A. Sidhu, P. Manchanda, R. Ahuja, 1,2,4-triazolyldithiocarbamate silver nano conjugate: potent seed priming agent against bakanae disease of rice (Oryzae sativa), Eur. J. Plant Pathol. 162 (2022) 825–841, https://doi.org/10.1007/s10658-021-02439-w.

[36] A. Raj, P. Shah, N. Agrawal, Dose-dependent effect of silver nanoparticles (AgNPs) on fertility and survival of Drosophila: an in-vivo study, PLoS One 12 (2017) e0178051, https://doi.org/10.1371/journal.pone.0178051.

[37] E.G. Wulff, J.L. Sørensen, M. Lübeck, K.F. Nielsen, U. Thrane, J. Torp, *Fusarium* spp. associated with rice Bakanae: ecology, genetic diversity, pathogenicity and toxigenicity, Environ. Microbiol. 12 (2010) 649–657, https://doi.org/10.1111/j.1462-2920.2009.02105.x.

[38] M. Haroon, A. Zaidi, B. Ahmed, A. Rizvi, M.S. Khan, J. Musarrat, Effective inhibition of phytopathogenic microbes by eco-friendly leaf extract mediated silver nanoparticles (AgNPs), Indian J. Microbiol. 59 (2019) 273–287, https://doi.org/10.1007/s12088-019-00801-5.

[39] Y.-K. Jo, W. Cromwell, H.-K. Jeong, J. Thorkelson, J.-H. Roh, D.-B. Shin, Use of silver nanoparticles for managing Gibberella fujikuroi on rice seedlings, Crop Protect. 74 (2015) 65–69, https://doi.org/10.1016/j.cropro.2015.04.003.

[40] Y. Jian, X. Chen, T. Ahmed, Q. Shang, S. Zhang, Z. Ma, Y. Yin, Toxicity and action mechanisms of silver nanoparticles against the mycotoxin-producing fungus Fusarium graminearum, J. Adv. Res. 38 (2022) 1–12, https://doi.org/10.1016/j.jare.2021.09.006.

[41] P.R. More, S. Pandit, A. De Filippis, G. Franci, I. Mijakovic, M. Galdiero, Silver nanoparticles: bactericidal and mechanistic approach against drug resistant pathogens, Microorganisms 11 (2023) 369, https://doi.org/10.3390/microorganisms11020369.
[42] S.A.J. Quazi, S. Meon, H. Jaafar, Z.A.B.M. Ahmad, The role of phytohormones in relation to bakanae disease development and symptoms expression, Physiol. Mol. Plant Pathol. 90 (2015) 27–38, https://doi.org/10.1016/j.pmpp.2015.02.001.
[43] P. Hedden, V. Sponsel, A century of gibberellin research, J. Plant Growth Regul. 34 (2015) 740–760, https://doi.org/10.1007/s00344-015-9546-1.
[44] W. Bao, T. Nagasaka, S. Inagaki, S. Tatebayashi, I. Imazaki, S. Fuji, T. Tsuge, M. Shimizu, K. Kageyama, H. Suga, A single gene transfer of gibberellin biosynthesis gene cluster increases gibberellin production in a *Fusarium fujikuroi* strain with gibberellin low producibility, Plant Pathol. 69 (2020) 901–910, https://doi.org/10.1111/ppa.13176.